

Research Article

Mechanism of Loading Fracture of Coal Mass and Formation of Oil and Gas Disaster Channel in Coal and Oil Resources Costorage Area

Yawu Shao ¹, Yonglu Suo ^{1,2} and Tao Yang ^{1,2}

¹School of Energy, Xi'an University of Science and Technology, Xi'an 710054, Shaanxi, China

²Key Laboratory of Department of Education of Western Mine Mining and Disaster Prevention, Xi'an University of Science and Technology, Xi'an 710054, Shaanxi, China

Correspondence should be addressed to Yawu Shao; syw1918@163.com

Received 2 October 2021; Revised 6 December 2021; Accepted 31 December 2021; Published 24 January 2022

Academic Editor: Yanbo Zhang

Copyright © 2022 Yawu Shao et al. This is an open access article distributed under the Creative Commons Attribution License, which permits unrestricted use, distribution, and reproduction in any medium, provided the original work is properly cited.

Fracture structure characteristics are crucial for determining the fracture mechanism of coal mass and the migration law of oil and gas disasters. In this study, computed tomography (CT) scanning technology and fractal theory were used to investigate the damage process of coal mass in the common storage area of coal and oil resources under uniaxial compression as well as the degree of damage of high-pressure oil and gas diffusion to the surrounding coal and rock mass. Uniaxial compression and acoustic emission signal acquisition tests of coal mass were conducted. The relationship among the load evolution law of coal samples at different positions around the oil well and the failure mode of key failure positions were further analyzed. Finally, the formation mechanism of coal load fracture and oil and gas disaster channel in coal and oil resource costorage area was investigated. The test results showed the following: (1) High-pressure oil and gas diffusion degrades the mechanical properties of coal mass in varying degrees. The closer the coal sample to the oil well, the greater the fracture development degree, the fracture density, the fracture fractal dimension of coal sample, and the severity of the coal mass damage and the lower the compressive strength, the acoustic emission event number, and the cumulative energy. (2) The lateral diffusion of high-pressure oil and gas changes the failure mode of coal samples in the common storage area of coal and oil resources. The failure modes when the sampling location is away from the oil well are step failure, conjugate shrinkage failure, and high-frequency vibration intermittent microcrack fracture. (3) Coal mass instability and coal mine oil and gas disaster in the common storage area of coal and oil resources can easily be induced by the formation of microfracture expansion, extension, and coalescence caused by coal failure, the formation of network and macrochannels of main fracture, and the instantaneous release of accumulated stress during failure.

1. Introduction

Shuangma coal mine is located in the costorage area of coal and oil resources in eastern Ningxia. Numerous abandoned oil wells from early oil exploitation produced the oil-bearing layer, resulting in the diffusion of high-pressure oil and reservoir gas into the coal seam and forming an oil and gas accumulation area around abandoned oil wells (Figure 1). The initiation, expansion, coalescence, expansion failure, and rapid release of accumulated stress of internal cracks in mining coal mass in this area [1] can easily induce dynamic disasters such as oil and gas disasters [2]. Fracture is the

migration channel of oil and gas, and it is an important factor for destroying mining coal mass and migrating oil and gas. Research on the load breaking of coal mass and formation mechanism of an oil and gas disaster channel in coal and oil resource costorage area is crucial for preventing and controlling oil and gas disasters in coal mines [3–5].

Rocks have a complex internal structure, making it challenging to accurately describe the fracture structure of coal and rock mass by direct measurement. As a nondestructive detection technology, computed tomography (CT) is not only used to characterize rock fractures, minerals, and pore permeability [6–8], but also used widely to characterize

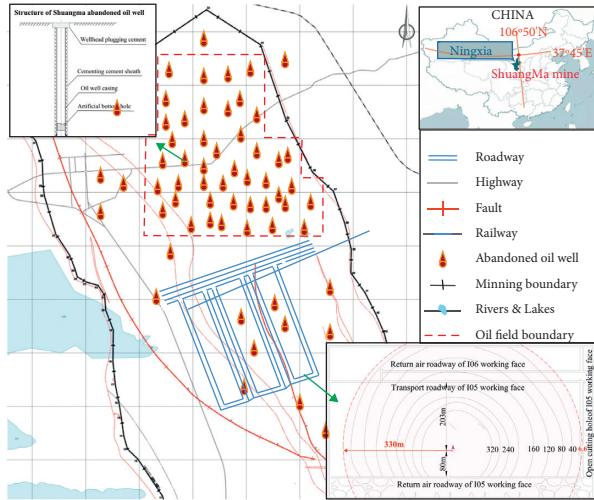


FIGURE 1: Oil and gas reservoir disasters in working face of Shuangma coal mine.

and quantitate rock internal pore structure [9]. Zhao [10] studied how mineral inclusions in coal influence its load failure. Ru [11] used CT scanning to investigate the distribution characteristics of minerals, pores, and fractures as well as the evolution characteristics of fracture network under stress. Kaide [12] studied the mechanical properties of uniaxial compression coal in different bedding directions. Jiang [13] studied how primary cracks affect the development and evolution of new cracks under different shear rates. In [14] pore and fracture development in coal under stress conditions are investigated based on NMR and fractal theory. Several scholars have studied the characteristics and laws of acoustic emission in the main fracture stage of coal. For example, Xiaoran [15] used parameters, such as acoustic emission counting, to describe the propagation process of prefabricated cracks in coal samples under compression. Moradian [16] used impact parameters to describe the stage evolution from microcrack formation to macrocrack cracking. However, a single-parameter analysis ignores other pieces of information in acoustic emission waveform and cannot fully reflect the precursory evolution characteristics of disasters. Hence, scholars have used multiparameter comprehensive analysis to study the precursory information and crack evolution characteristics of coal and rock mass failure under different loading paths [17–20]. Ohtsu [21] categorized acoustic emission events in uniaxial compression coal and rock mass into tension and shear types crack events based on waveform characteristics and the relationship among rise time peak amplitude and count duration ratios (RA-AF).

Previous studies on the damage of coal and rock mass have focused on the effects of mineral impurities and bedding dip angle on the strength and anisotropy of coal and rock mass under uniaxial compression. However, only few studies have investigated the evolution characteristics of RA-AF cracks under uniaxial compression as well as the formation mechanism of oil and gas disaster migration channel when coal mining damage occurs. Hence, this study used coal sample CT scanning technology and acoustic emission

test to analyze the influence of fracture structure on the failure mode of coal mass. This study also explored the failure mode of coal mass damaged by high-pressure oil and gas at different positions of abandoned oil wells; we further investigated the mechanism of coal mass load fracture and oil and gas disaster migration channel in the common storage area of coal and oil resources.

2. Experimental Design

2.1. Preparation of Coal and Rock Mass Specimens. The coal samples used in the test were Jurassic coal from I05 working face of coal seam 4⁻¹ of Shuangma coal mine in Ningdong mining area. Sand lines were used to place the coal samples 50 m, 150 m, and 300 m away from the abandoned oil well (near, middle, and edge of the well, respectively). This placement variety was because the acoustic emission probe easily falls after the loading and fracture of a cylindrical coal sample. When the acoustic emission probe falls, the monitoring data become deficient. However, sufficient monitoring data are needed to intuitively describe the surface damage of coal mass, avoid the secondary damage of cutting to coal mass, and reduce experimental error. The coal lump was cut into three 100 mm³ coal samples, and a typical coal sample at each position was selected for analysis. With the oil well as the origin, the numbers from near to far were C₁, C₂, and C₃. CT scanning was conducted to determine the influence of high-pressure oil and gas on the fracture characteristics, failure mode of coal mass in the common storage area of kerosene resources, and the formation law of oil and gas disaster migration channel.

2.2. Experiments. An X-ray spiral CT machine (UTC780, Lianying Medical Technology Co., Ltd) was used to analyze the influence of high-pressure oil and gas diffusion on the fracture characteristics of coal samples at different positions.

The uniaxial compression test was conducted on a rock mechanics test system (RMT-150). The displacement loading control was adopted. To avoid the noise signal caused by the friction and slip of the coal sample at the initial loading stage, the coal sample was preloaded to 2 kN; the sample was then loaded at a rate of 0.2 mm/min until the coal sample was damaged.

To monitor the macrofracture of coal mass during loading, a high-speed camera was used to take real-time photographs of the coal sample loading, and an acoustic emission probe was set on both sides and rear side of the coal sample. A DS5-16B full information acoustic emission signal analyzer was used to monitor the acoustic emission information during the entire uniaxial compression test in real time. To reduce the impact of static electricity and noise on acoustic emission test, the acoustic emission system and testing machine were grounded, and the monitoring threshold was set to 38 dB. Grease was applied between the probe and the coal sample to enhance the coupling effect. Before the test, the coal sample analog signal source was knocked, the channel response of each probe was observed, and each probe was confirmed normal (Figure 2).

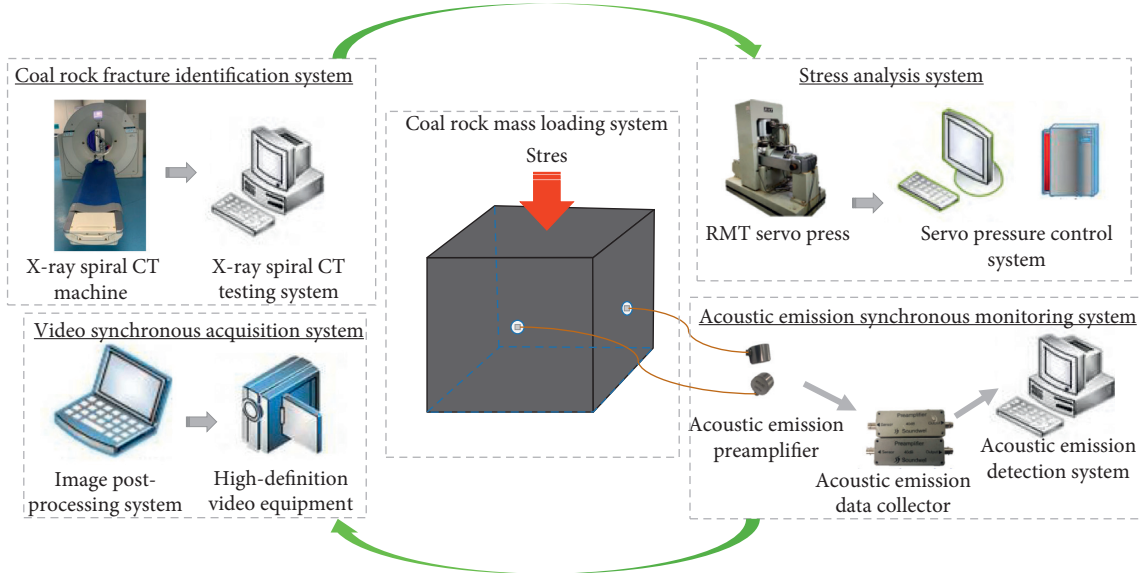


FIGURE 2: Experiment system.

3. Test Results

3.1. Accurate Identification of Fracture Parameters. The CT slice thickness of the coal samples was set to 2 mm, and 50 CT slice images were obtained for a single coal sample. Considering space limitation, photographs at 2, 4, 6, 8, and 10 cm positions were selected for each coal sample to reflect the fracture distribution characteristics of the whole coal sample. The coupling algorithm of fracture binarization and adjacent point interpolation was established, and the command was written in MATLAB to binarize the image [22].

According to the results of CT slice processing and fracture characteristic analysis of coal samples (Table 1), when the coal samples are close to the oil well, the distribution, opening and penetration degree, and fracture density of fractures increase. This trend indicates the damage of high-pressure oil and gas diffusion to the surrounding coal body and provides an internal medium to accumulate oil and reservoir gas.

3.2. Characteristics of Stress and Strain and Acoustic Emission of Loaded Coal and Rock Mass. To avoid several acoustic emission low-energy damage signals that affect the damage of key signals during coal sample loading, the characteristic signal of damage and fracture of coal and rock mass was selected using the signal energy contribution rate. The collected signal $s_i (1 \leq i \leq n)$ was regarded as a whole S , $S = [s_1, s_2, s_3, \dots, s_{n-1}, s_n]$, where the signal s_i detected in rock damage and fracture carries energy e_i , and the energy monitored in the whole failure process is $E = [e_1, e_2, e_3, \dots, e_{n-1}, e_n]$.

The cumulative energy contribution rate is calculated using the frequency $f_i (i = 1, 2, 3, \dots, n)$ corresponding to the calculated energy after the descending arrangement of different energy contribution rates in the process of damage and fracture β_i :

$$\beta_i = \frac{\sum_{k=1}^i e_k f_k}{\sum_{k=1}^n e_k f_k} \quad (i = 1, 2, 3, \dots, n). \quad (1)$$

Statistically, if a certain phenomenon is regular, its statistical probability will exceed 85%. During rock damage and fracture, the energy carried by the acoustic emission monitoring signal may differ because of its own anisotropy. Therefore, the average value of the signal energy for the screening energy contribution rate between 85% and 95% was used as the initial selection threshold Q , and the final selection threshold was Q_s . The calculation formula is [23]

$$Q = \left\{ \sum_{i=1}^n \frac{e_i}{n}; e_i \in E, 0.85 \leq \beta_i \leq 0.95 \right\}, \quad (2)$$

$$Q_s = \max E \cdot R^2 + Q,$$

where $\max E$ represents the maximum energy value of the monitored acoustic emission signal and R represents the ratio of the number of signals after the energy exceeds the preliminary selection threshold.

Based on the total stress-strain curve of rock under uniaxial compression, the deformation process of Shuangma coal sample was divided into four stages: initial pore compaction (stage I), elastic deformation (stage II), rapid fracture development (stage III), and post-peak (stage IV) [24, 25].

In the loading process, the elastic modulus of coal mass changed rapidly in the rapid fracture stage. Thus, the crack expanded and fractured violently, which is similar to the dynamic disaster of coal seam mining. Therefore, stress-strain curve rapid fracture stage was selected to analyze the rapid fracture mechanism. Figure 3 illustrates the trend of stress, strain, ringing count, characteristic energy signal, and energy accumulation with time during loading:

TABLE 1: CT slice processing and fracture characteristics analysis of coal samples.

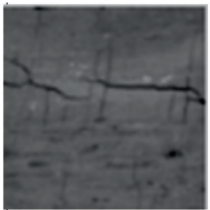
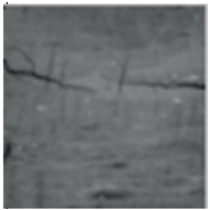
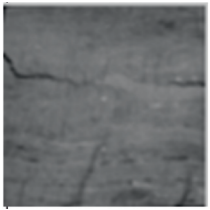

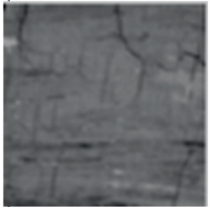





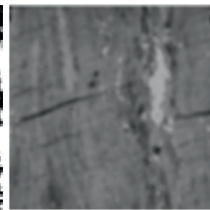
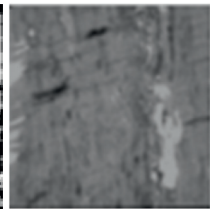
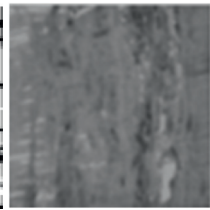
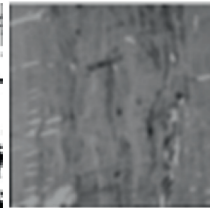
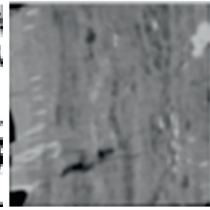


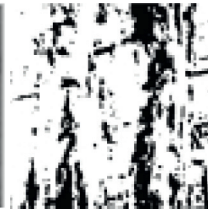
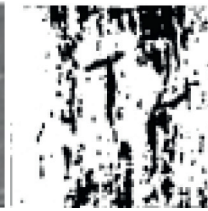

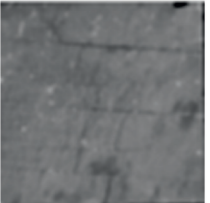
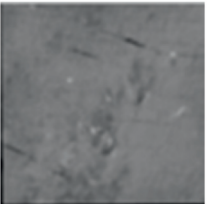
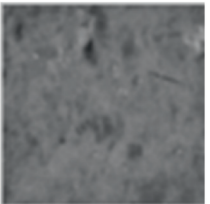
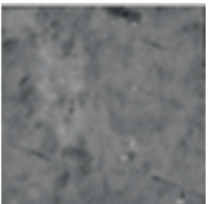
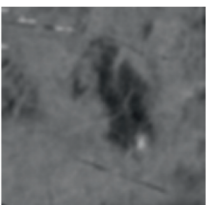



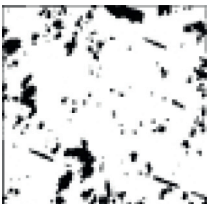

Samples	Picture type	2 cm	4 cm	6 cm	8 cm	10 cm	Fracture characteristics
C ₁	CT section						<p>The fracture types are complex, the main fractures are developed, and the microfractures are many, especially the two main fractures longitudinally distributed in the middle. These major fractures are approximately 60 mm long and greater than 60 mm in depth, and the opening is 2 mm.</p>
	Binary graph						
C ₂	CT section						<p>Microfractures are developed, and the number of fractures gradually decreases from the edge to the middle. An obvious intersection can be observed between the vertical (strip in binary image) and the fractures mainly in the direction of parallel slices (schistose in binary image).</p>
	Binary graph						

TABLE 1: Continued.

Samples	Picture type	2 cm	4 cm	6 cm	8 cm	10 cm	Fracture characteristics
C ₃	CT section						The coal mass is relatively complete, and microfractures are sporadically distributed. Occasionally, cracks with long trace length appear, but the depth is small.
	Binary graph						

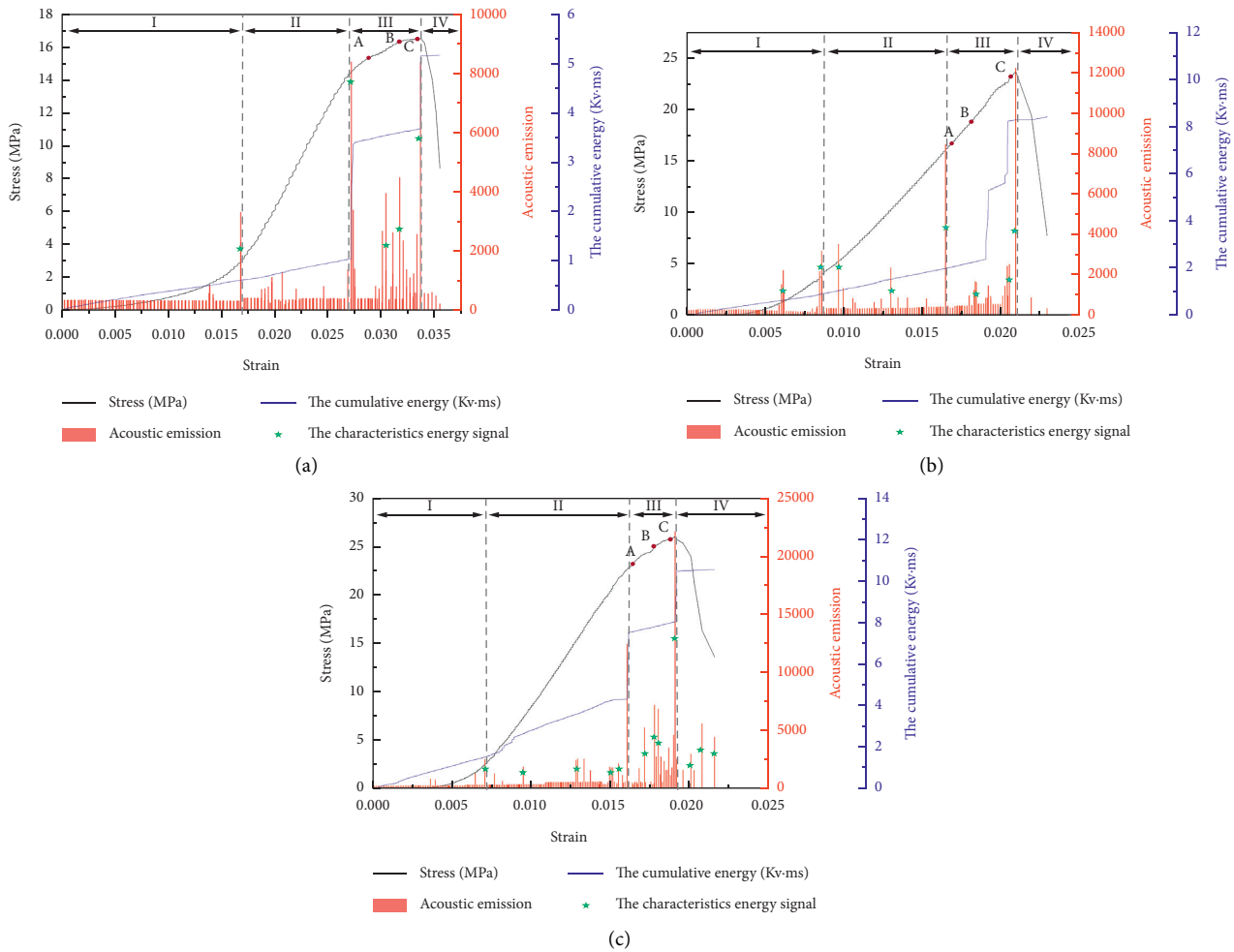


FIGURE 3: Different coal mass stress-strain and acoustic emission parameters characteristic signals. (a) Sample C₁, (b) sample C₂, and (c) sample C₃.

- (1) Fracture compaction (stage I; stress level, 0–20%): in this stage, the internal cracks of coal mass were compacted and closed, the stress-strain curve was concave, oil and gas gathered in the coal in the form of independent cracks, and the storage capacity decreased with the closure of cracks. As the fracture density (quantity and trace width) of coal samples at different positions increased, the acoustic emission ringing count, cumulative energy, and ability to store oil and gas increased.
- (2) Elastic deformation (stage II; stress level, 20%–90%): in this stage, the original cracks compacted further and new cracks developed. The stress-strain relationship of coal mass was approximately a linear positive correlation. The acoustic emission ring count was relatively stable, and the cumulative energy curve increased rapidly. Oil and gas diffused regionally as cracks developed.
- (3) Rapid fracture (stage III; stress level 90%–100%): the cracks rapidly expanded to form a network structure and finally penetrated the whole coal sample to form

a macrofracture. The stress, elastic modulus, ring count, and cumulative energy increased rapidly. At this stage, the network structure and macrofracture produced several storage and migration channels for oil and gas. The acoustic emission signals of coal samples at different positions and the storage and migration capacity of oil and gas increased with increasing fracture density.

- (4) Post-peak (stage IV): the coal mass formed a through main failure surface, and the bearing capacity decreased rapidly to a certain value. The acoustic emission ringing count decreased rapidly and remained at an extremely low level, and the accumulated energy remained unchanged. The generation of through failure surface in this stage promoted the formation of a macrochannel of oil and gas disasters.

Table 2 illustrates that, compared with the C₃ coal sample far from the oil well, the compressive strength and cumulative energy of the C₂ coal samples located in the medial position of the influence of oil and gas diffusion decreased by

TABLE 2: Compressive strength and acoustic emission energy of different specimens.

Sample number	C ₁	C ₂	C ₃
Compressive strength/MPa	16.59	23.46	26.72
Accumulated energy/kV·ms	5.21	8.41	11.065
Number of AEs at complete rupture/Pcs	51405	70852	90395
Characteristic energy at peak/V·ms ⁻¹	1875.65	1949.27	2597.93

13.90% and 31.57%, respectively; the acoustic emission energy and the number of events during a complete fracture of coal mass were reduced by 33.28% and 27.58%, respectively. The compressive strength and cumulative energy of C₁ coal samples near the oil well decreased by 61.06% and 112.38%, and the acoustic emission energy and the number of events decreased by 38.51% and 75.85%, respectively, when the coal mass was completely broken.

The degree of coal mass damage caused by high-pressure oil and gas diffusion increased with the sampling location close to the oil well, which significantly reduced the compressive strength, cumulative energy, and the number of fracture events of coal mass. The deterioration of the mechanical properties of coal mass was suitable for the formation of oil and gas storage and migration channels.

4. Discussion

4.1. Fractal Characteristics of Cracks. Based on the theory of the fractal characteristics of fractured rock mass [26], the fractal box counting method was used to calculate the fractal dimension of primary fractures. The linear fitting function of the typical box counting method for calculating the degree of crack distribution in coal and rock specimens is [27]

$$\text{Log } N(\delta) = -D \log \delta + C, \quad (3)$$

where C is constant and D is the fractal dimension of coal specimens.

Figure 4 shows the fractal dimension characteristics of coal sample fracture structure at different positions. The coal sample fracture structure had a significant impact on its fractal dimension. The fractal dimensions of C₁, C₂, and C₃ coal samples were 1.8370, 1.6503, and 1.5192, respectively. As the coal sample was far from the oil well, its fractal dimension increased by 11.13% and 20.92%, respectively.

The analysis of the CT scanning results of the coal mass showed that the closer the sampling position to the oil well, the greater the extension length, opening degree, and depth of the main fractures of the coal sample; likewise, the greater the number of fractures and fractal dimension, the greater the damage degree of high-pressure oil and gas diffusion to the coal sample, and the easier it is to form a macro gas channel under load.

4.2. Analysis of the Failure Evolution. The damage stress wave monitored by acoustic emission is a continuous aperiodic waveform induced by the fracture at different times. As shown in Figure 5, any wave function can be

decomposed into sinusoidal functions with different amplitude frequencies [28].

Therefore, each damage fracture energy event can be characterized as a sinusoidal function. The frequency spectrum chart of the damage waveform after Fourier transform was characterized by the frequency and amplitude of each damage fracture. This was aimed to deduce damage fracture in the rapid fracture stage.

The fracture modes of coal mass under load can be divided into tensile and shear failures. Tensile failure leads to lateral tensile expansion of crack and the signal exhibited characteristics of high frequency and low amplitude. Shear failure led to friction dislocation up and down the shear plane, and the signal exhibited characteristics of low frequency and high amplitude [29]. Ohno and Ohtsu [30] developed a method for describing fractures in concrete. This method only uses relative amplitude values adequate to resonant acoustic sensors, unlike moment tensor inversion methods or those using the direction of the first motion. According to [31], the damage evolution relationship of coal samples was established based on the time sequence of damage deterioration of characteristic signals obtained from waveform and spectrum analysis. The damage types of characteristic signals at the marked key positions in Figure 3 are shown in Table 3.

Figure 6 illustrates the RA-AF relationship of coal samples from Shuangma mine. With the sampling location away from the oil well, the number of C₂ and C₃ fractures of coal samples increased by 40.62% and 81.93%, respectively, and the number of tensile failures was significantly higher than that of shear failure. These observations indicate that the closer the coal mass to the oil well, the greater the damage degree of high-pressure oil and gas diffusion, the smaller the number of coal sample fracture events, the more complex the failure mode, and the greater the oil and gas storage and migration ability.

Figure 7 illustrates the macrofracture characteristics of the key failure positions of the coal sample in the rapid fracture stage (III); the figure also illustrates the analysis of the fracture signal of coal mass corresponding to RA-AF. At the initial stage of loading failure (A), the coal sample C₁ near the oil well passed through under the shear action of two longitudinal main fractures. Meanwhile, the coal sample loading compressive stress and energy were still in the accumulation state. Although the fractures passed through, the overall structure was not completely damaged. The final fracture of the coal sample was induced by the middle shear stress (B), and the combined action of tension and shear failure (C) led to the rapid release of the stress accumulated by the overall disintegration of the coal sample. This stress release was because the original

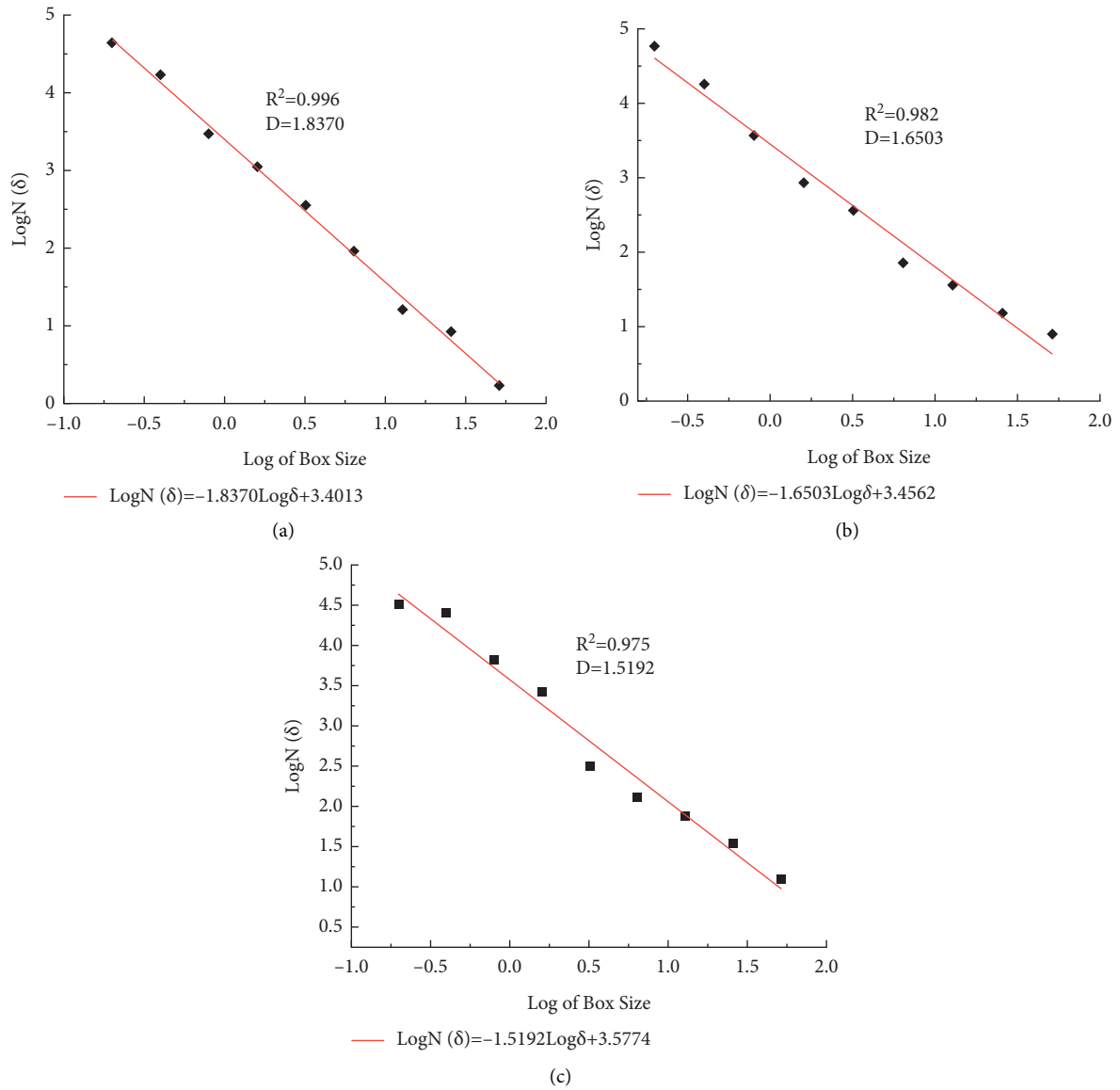


FIGURE 4: Calculation of fractal dimension of coal sample crack based on the fractal dimension method. Calculation of crack dimension of (a) C₁ coal sample, (b) C₂ coal sample, and (c) C₃ coal sample.

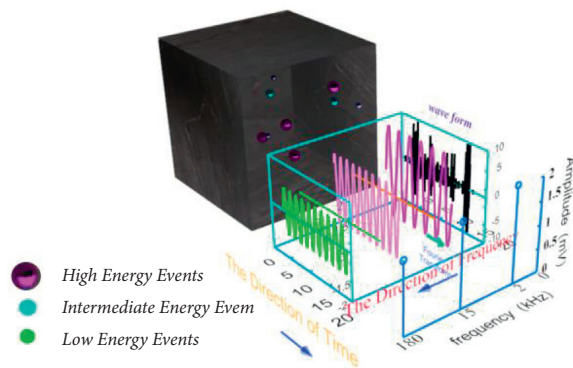


FIGURE 5: Deduction of the acoustic emission spectrum at the rupture stage.

TABLE 3: Key location feature signal damage types.

Sample number	Energy characteristic signal		
	A	B	C
C ₁	Shear	Mixed	Mixed
C ₂	Tensile	Mixed	Shear
C ₃	Tensile	Tensile	Mixed

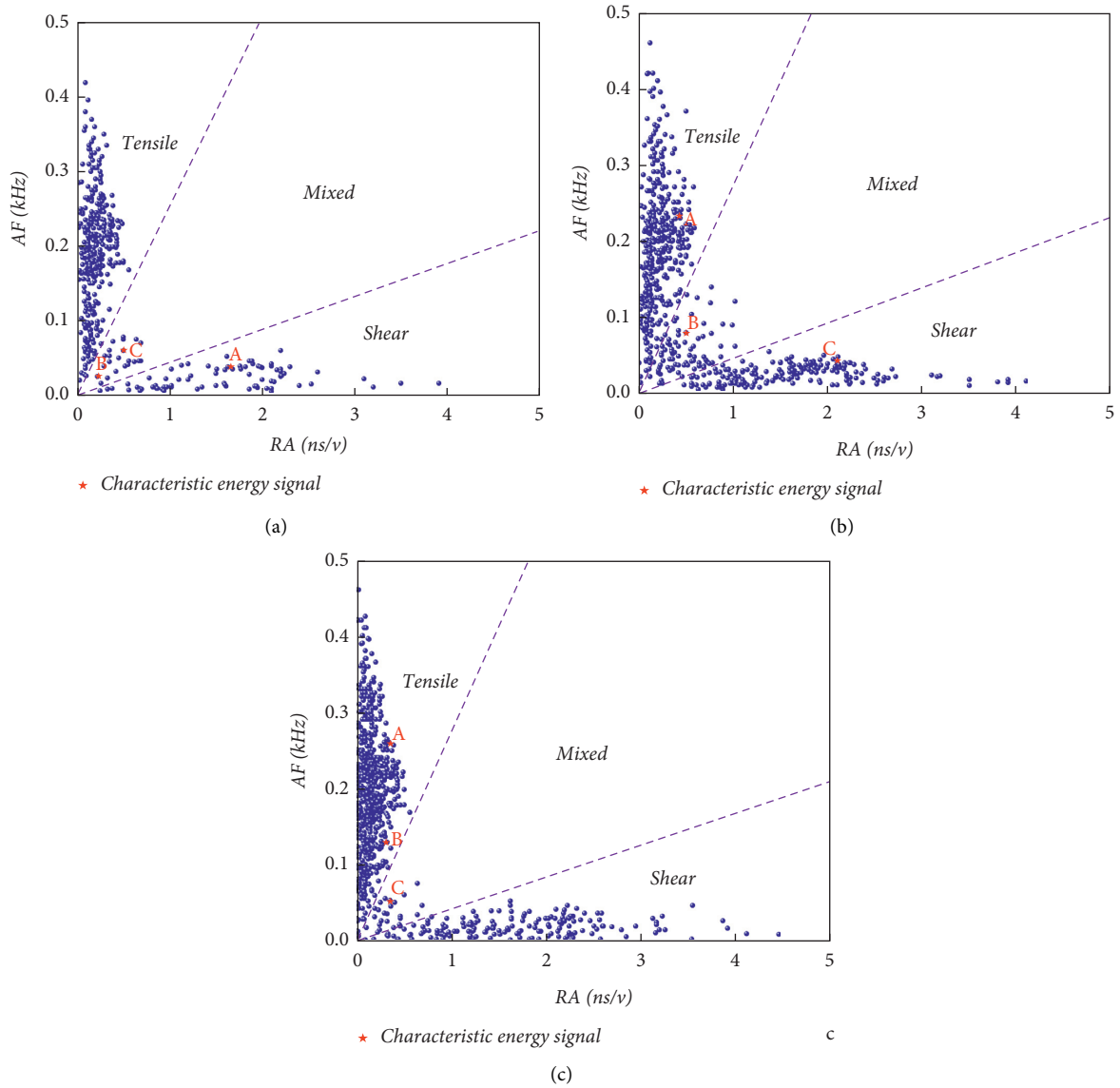


FIGURE 6: RA-AF damage analysis of different coal masses. (a) Sample C₁. (b) Sample C₂. (c) Sample C₃.

fracture surface with large extension length and cutting depth in the coal mass first produced a shear failure surface along the direction of the original large fracture surface in the loading process. For C₂ coal samples at the middle of the oil and gas diffusion influence, the coal and rock mass showed a composite failure accompanied by tensile failure and shear failure at the initial stage of

loading failure (A) in the rapid fracture stage. As loading strength increased, the cracks in the coal deformed, expanded, and penetrated, forming a crack network. Finally, the cracks in the middle of the fracture were completely destroyed at the stress peak (C) under the induction of shear failure (B); the cracks in the specimen were gradually destroyed from the edge, which is similar to

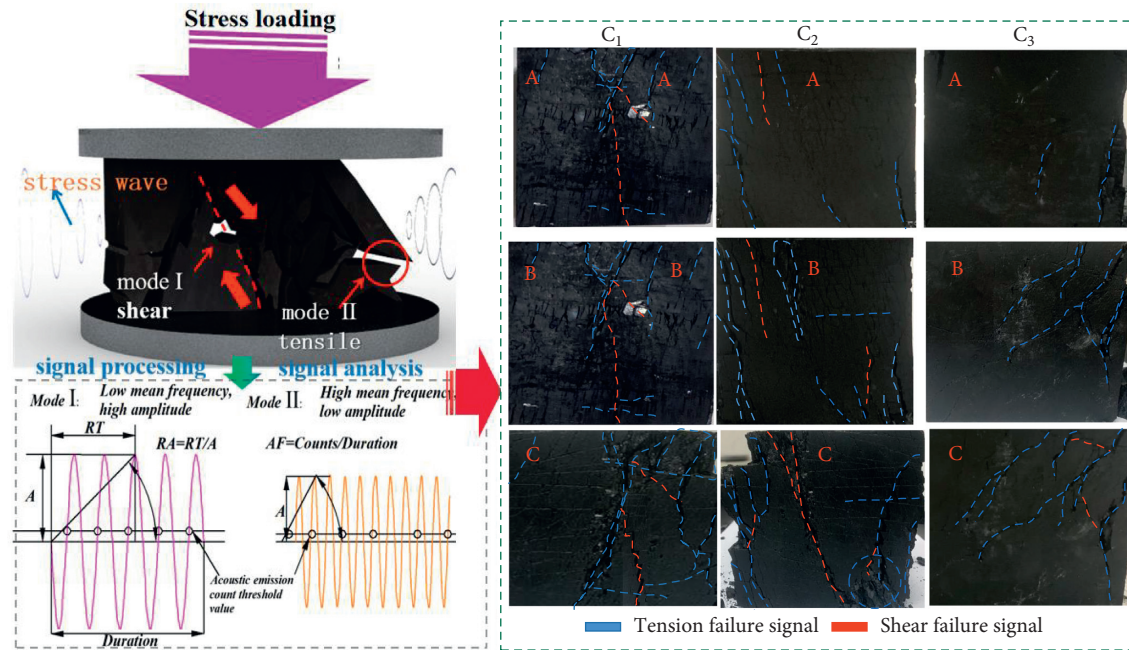


FIGURE 7: Coal mass fracture analysis.

conjugate failure. At the initial stage of the loading failure (A) of the edge coal sample C_3 , tension failure occurred at the edge of the coal mass. As the loading strength increased, fracture deformation expanded and penetrated, forming a fracture network. The final fracture was induced by central shear failure (B), resulting in stress release accumulated by coal and rock mass disintegration (C) under the combined action of tension and shear failure. Moreover, the residual strength of coal mass after yield strength was high.

At the initial stage of the loading failure of coal samples, tension failure led to fracture expansion, forming an independent fracture structure; moreover, the fracture density increased, resulting in the accumulation of high-pressure oil and gas into the coal mass. When loading to the yield strength, the shear failure increased gradually, and the initial fracture extension and the new fracture germination led to the rapid cross expansion of the fracture to form a network structure. The fracture structure was in a good conduction state in the region and in a poor conduction state among regions. Meanwhile, the oil and gas concentration in the coal mass increased rapidly. When loaded to the ultimate strength, the fracture was developed to run through the whole coal sample, and the generation of a macrochannel of oil and gas led to the diffusion of a large amount of oil and gas to the mining face, causing an oil and gas disaster. The stress and energy accumulated by the final overall disintegration of the coal body were rapidly released, which can easily induce the dynamic disaster of oil and gas gushing out of coal mines in the overlapping area of coal and oil resources. Therefore, the fracture evolution and failure form of coal and rock mass in the costorage area of coal and oil resources are crucial to oil and gas disaster prevention technology in this coal and oil resources costorage area of coal mine.

5. Conclusion

- (1) The damage degree of high-pressure oil and gas diffusion to the surrounding coal sample was linearly and negatively correlated with the oil well distance. The closer the coal sample to the oil well, the greater the fracture development degree, fracture density, and fractal dimension. CT scanning results showed that the maximum reduction of fractal dimension of coal sample was 20.92% when the sampling location was away from the oil well.
- (2) The diffusion of high-pressure oil and gas degraded the mechanical properties of coal samples to varying degrees and reduced the energy released during damage. With the sampling location away from the oil well, the maximum increase in coal sample compressive strength and cumulative energy was 61.06% and 112.38%, respectively, and the maximum increase in fracture number at the key fracture location was 81.93%.
- (3) The lateral diffusion of high-pressure oil and gas changed the failure mode of coal samples. With the sampling location away from the oil well, the failure modes are as follows. The new fractures of coal samples near the oil well propagated along the main fractures in a step-by-step manner; conjugate shrinkage failure was caused by the low-frequency continuous vibration of the medial position in the coal sample. Three forms of fracture were caused by high-frequency vibration intermittent in micro-cracks of edge coal samples.
- (4) In the loading process of coal mass, tension failure promoted the expansion, extension, and coalescence of fractures; shear failure promoted the generation of

new fractures between the original main fractures, resulting in the rapid cross expansion and penetration of a fracture network structure. Each stage was accompanied by the migration, accumulation, diffusion, and emission of oil and gas in the coal as well as the rapid release of stress accumulated by the final disintegration of coal mass. It was easy to induce coal mass instability, oil and gas, and other dynamic disasters in the common storage area of coal and oil resources.

Data Availability

The data analyzed or generated during the research can be provided by the corresponding author upon request.

Additional Points

Based on the research on the failure and instability of coal mass and the prevention and control of oil and pneumatic disasters in Shuangma coal mine in Ningxia coal and oil resources costorage area, this paper mainly studies mechanism of loading fracture of coal mass and formation of oil and gas disaster channel in coal and oil resources costorage area.

Conflicts of Interest

The authors declare that they have no conflicts of interest.

References

- [1] J. Yiwen, L. Kray, L. Xiaoshi et al., "Micro-structural evolution and their effects on physical properties in different types of tectonically deformed coals," *International Journal of Coal Science & Technology*, vol. 1, no. 3, pp. 264–275, 2014.
- [2] Y. Suo, Y. Liu, X. Jiang et al., "Evaluation on the influence of abandoned oil wells on the safety mining of coal seams," *Journal of Xi'an university of Science and Technology*, vol. 39, no. 05, pp. 753–760, 2019.
- [3] H. John and A. Harrison, *Engineering Rock Mechanics Introduction to the Principles*, Elsevier Science, vol. 55, no. 2, p. 72, St. Louis and New York, 2002.
- [4] L. Scholtès, F. V. Donzé, and M. Khananal, "Scale effects on strength of geomaterials, case study: Coal," *Journal of the Mechanics and Physics of Solids*, vol. 59, no. 5, pp. 1131–1146, 2011.
- [5] N. Tsafnt, N. Amana, and A. S. Jones, "Analysis of coke under compressive loading: a combined approach using micro-computed tomography, finite element analysis, and empirical models of porous structures," *Fuel*, vol. 90, no. 1, pp. 384–388, 2011.
- [6] M. Van Geet and R. Swennen, "Quantitative 3D-fracture analysis by means of microfocus X-Ray Computer Tomography (μ CT): an example from coal," *Geophysical Research Letters*, vol. 28, no. 17, pp. 3333–3336, 2001.
- [7] Y. Jing, R. T. Armstrong, H. L. Ramandi, and P. Mostaghimi, "Coal cleat reconstruction using micro-computed tomography imaging," *Fuel*, vol. 181, pp. 286–299, 2016.
- [8] C. Ö. Karacan and E. Okandan, "Fracture/cleat analysis of coals from Zonguldak Basin (northwestern Turkey) relative to the potential of coalbed methane production," *International Journal of Coal Geology*, vol. 44, no. 2, pp. 109–125, 2000.
- [9] S. Xiaoxia, T. Yuegang, L. Wei et al., "Advanced quantitative characterization of seepage pores of deformed coals based on micro-CT," *Journal of China Coal Society*, vol. 38, no. 3, pp. 435–440, 2013.
- [10] Y. Zhao, G.-F. Zhao, and Y. Jiang, "Experimental and numerical modelling investigation on fracturing in coal under impact loads," *International Journal of Fracture*, vol. 183, no. 1, pp. 63–80, 2013.
- [11] Z. Ru, A. Ting, L. Hegui, Z. Zetian, and L. Jianfeng, "3D reconstruction method and connectivity rules of fracture networks generated under different mining layouts," *International Journal of Mining Science and Technology*, vol. 23, no. 6, pp. 863–871, 2013.
- [12] L. Kaide, L. Quansheng, Z. Yuanguang, and L. Bin, "Experimental study of coal considering directivity effect of bedding plane under Brazilian splitting and uniaxial compression," *Chinese Journal of Rock Mechanics and Engineering*, vol. 32, no. 2, pp. 308–316, 2013.
- [13] X. Jiang, C. Lichao, T. Haoyue, and L. Wang, "Effects of original cracks on macro-meso evolution law of coal shear failure," *Chinese Journal of Rock Mechanics and Engineering*, vol. 32, no. 1, pp. 33–40, 2013.
- [14] Y. Zhao, C. Wang, N. Lin, H. Zhao, and B. Jing, "Pore and fracture development in coal under stress conditions based on nuclear magnetic resonance and fractal theory," *Fuel*, vol. 309, Article ID 122112, 2022.
- [15] X. Wang, E. Wang, L. Xiao-Fei, and X. Li, "Macro-crack propagation process and corresponding AE behaviors of fractured sandstone under different loading rates," *Chinese Journal of Rock Mechanics and Engineering*, vol. 37, no. 6, pp. 1446–1458, 2018.
- [16] Z. Moradian, H. H. Einstein, and G. Ballivy, "Detection of cracking levels in brittle rocks by parametric analysis of the acoustic emission signals," *Rock Mechanics and Rock Engineering*, vol. 49, no. 3, pp. 785–800, 2016.
- [17] Q. Liu, W. Lai, F. Lei et al., "Experimental study on damage strength of crack initiation and evaluation of brittle parameters of sandstone," *Chinese Journal of Geotechnical Engineering*, vol. 40, no. 10, pp. 1782–1789, 2018.
- [18] Y. Cong, F. Xia-ting, Y. Zheng, and Z. Q. Wang, "Experimental study on acoustic emission failure precursors of marble under different stress paths," *Chinese Journal of Geotechnical Engineering*, vol. 38, no. 7, pp. 1193–1201, 2016.
- [19] Z. Zhou, L. Guo-nan, N. Shu-li et al., "Acoustic emission characteristics and failure mechanism of high-stressed rocks under lateral disturbance," *Chinese Journal of Rock Mechanics and Engineering*, vol. 33, no. 8, pp. 1720–1728, 2014.
- [20] Y. Gu, Z. Wang, L. Qing-miao et al., "Laboratory study on RA value fractal feature of shale acoustic emission under conventional triaxial compression," *Journal of Chongqing University*, vol. 41, no. 2, pp. 78–86, 2018.
- [21] M. Ohtsu, T. Isoda, and Y. Tomoda, "Acoustic emission techniques standardized for concrete structures," *Journal of Acoustic Emission*, vol. 25, pp. 21–32, 2007.
- [22] H. Sun, *Study and Application of Stress Fracture Seepage Coupling Mechanism of Mining Coal and Rock*, Xi'an University of science and technology, China, Shaanxi, 2017.
- [23] Y. Xu-Long, Z. Yan-Bo, L. Xiang-Xin et al., "Optimization method for key characteristic signal of acoustic emission in rock fracture," *Rock and Soil Mechanics*, 2018.
- [24] M. Cai, M. He, and D. Liu, *Rock Mechanics and Engineering*, Xue Publishing House, Beijing: families, Second edition, 2013.
- [25] X. Lai, S. Zhang, F. Cui, Z. Wang, and H. Xu, "Fang Xianwei Energy release law and key disaster acoustic emission signal

- pickup during damage evolution of water bearing coal and rock,” *Journal of rock mechanics and engineering*, vol. 39, no. 03, pp. 433–444, 2020.
- [26] H. P. Xie, “The fractal effect of irregularity of crack branching on the fracture toughness of brittle materials,” *International Journal of Fracture*, vol. 41, no. 4, pp. 267–274, 1989.
- [27] Q. Z. Wang, S. Zhang, and H. P. Xie, “Rock dynamic fracture toughness tested with holed-cracked flattened Brazilian discs diametrically impacted by SHPB and its size effect,” *Experimental Mechanics*, vol. 50, no. 7, pp. 877–885, 2010.
- [28] X. Lai, J. Ren, F. Cui et al., “Study on vertical cross loading fracture of coal mass through hole based on AE-TF characteristics,” *Applied Acoustics*, 2020.
- [29] Y. Zhao, C. Wang, M. Teng, and B. Jing, “Observation on microstructure and shear behavior of mortar due to thermal shock,” *Cement and Concrete Composites*, vol. 121, no. 9, Article ID 104106, 2021.
- [30] K. Ohno and M. Ohtsu, “Crack classification in concrete based on acoustic emission,” *Construction and Building Materials*, vol. 24, pp. 2339–2346, 2010.
- [31] C. Balland, J. Billiotte, B. Tessier et al., “Acoustic monitoring of a thermo-mechanical test simulating withdrawal in a gas storage salt cavern,” *International Journal of Rock Mechanics and Mining Sciences*, vol. 111, pp. 21–32, 2018.